*Int. J. Solids Structures* Vol. 26, No. 4, pp. 483–495, 1990
Printed in Great Britain.

0020–7683/90 $3.00 + .00


# LARGE STRAIN ANALYSIS FOR PLASTIC-ORTHOTROPIC TUBES

DAVID DURBAN and MICHAEL KUBI†
Faculty of Aerospace Engineering, Technion—Israel Institute of Technology,
Haifa 32000, Israel

(*Received* 22 *February* 1989; *in revised form* 22 *June* 1989)

**Abstract**—A finite strain analysis is presented for internally pressurized rotating tubes. Material behaviour is governed by an elastoplastic flow theory associated with an orthotropic yield function due to Hill. The deformation pattern is restricted by the neglect of elastic compressibility and by the plane strain constraint, but allows for arbitrary strain hardening. That model includes the isotropic Mises and Tresca solids as particular cases. An exact quadrature type solution is given for the field equations. Comparison with experimental results for the bursting pressure of aluminum and copper tubes suggests an improvement when plastic orthotropy is accounted for. Some further analytical results are derived for thin walled tubes, elastic/perfectly-plastic solids, and for the small strain behaviour of elastic/linear-hardening tubes.

## INTRODUCTION

It is now widely recognized that plastic orthotropy, induced by the presence of a stress field within the material, is an important factor in the analysis of solid structures, particularly in the large strain range. In this work we address the classical problem of a thick-walled tube subjected to internal pressure $p$ and to inertia forces that result from rotation at an angular speed $\omega$. The study is for an elastoplastic material whose constitutive equation is derived from a flow theory associated with an orthotropic yield function introduced by Hill (1976). The deformation pattern is restricted by assuming axially-symmetric plane-strain conditions and neglecting elastic compressibility. Otherwise, the analysis is fairly general in considering finite strains and allowing for arbitrary hardening characteristics.

The mathematical model, presented in the next section, is reduced to a system of two transcendental equations with the values of the effective stress at the boundaries as unknowns. The treatment proceeds here along the lines of the investigation in Durban (1979), where the pressurized tube problem has been solved, within the context of finite elastoplasticity, for an incompressible Mises solid. That analysis has been extended later by Lo and Abeyaratne (1981) for the rotating tube. In the present study we recover the isotropic Tresca and Mises models as particular cases.

The standard thin-wall approximation is employed to facilitate simple expressions for the failure lines and the performance envelope of the tube. These formulae reflect in a simple way the influence of plastic orthotropy in the presence of strain hardening.

A comparison with experimental data by Larsson *et al.* (1982), for the bursting pressure of aluminum and copper tubes, shows a nice agreement for a proper choice of the orthotropy parameter. The theoretical predictions were calculated here from the fully nonlinear equations.

The paper concludes with some further analytical results for elastic/perfectly-plastic solids, and for the small strain behaviour of elastic/linear-hardening materials.

## THE MATHEMATICAL MODEL

A thick walled tube is expanding in an axially symmetric pattern under the combined loading of internal pressure $p$ and rotation at angular speed $\omega$. The deformation field is constraint by the plane strain condition and elastic compressibility is neglected. Thus, with

† This work is based on a part of a Thesis to be submitted to the Technion, in partial fulfillment of the requirements for the degree of Master of Science.

$(r, \theta, z)$ standing for the usual undeformed material coordinates we have the finite strain components

$$\varepsilon_r = \ln(1+u') \quad \varepsilon_\theta = \ln\left(1+\frac{u}{r}\right) \tag{1}$$

where $u = u(r)$ is the radial displacement and the prime denotes differentiation with respect to $r$. Inserting relations (1) in the incompressibility constraint

$$\varepsilon_r + \varepsilon_\theta = 0 \tag{2}$$

results in the differential equation

$$\left(1+\frac{u}{r}\right)(1+u') = 1 \tag{3}$$

with the solution

$$u = \sqrt{r^2+C} - r \tag{4}$$

where $C$ is an integration constant. Combining the radial displacement profile (4) with the second of (1) we obtain a helpful differential connection

$$\frac{dr}{r} = \left(\frac{e^{\varepsilon_\theta}}{e^{-\varepsilon_\theta} - e^{\varepsilon_\theta}}\right) d\varepsilon_\theta \tag{5}$$

which will be used later in the analysis. Notice that the kinematic derivation so far is universally valid for all incompressible materials regardless of any particular constitutive equation.

Material behaviour is modelled, in the present study, by an elastoplastic flow theory which is based on an orthotropic yield function suggested by Hill (1976). The effective stress is defined by

$$\sigma_e^2 = \left(\sigma_z - \frac{\sigma_r+\sigma_\theta}{2}\right)^2 + \frac{3}{4\lambda^2}(\sigma_r-\sigma_\theta)^2 \tag{6}$$

where $(\sigma_r, \sigma_\theta, \sigma_z)$ are the usual Cauchy stress components and $\lambda$ is a material parameter that controls the relative contribution of the in-plane shear stress. As it stands, family (6) contains just one isotropic member given by $\lambda = 1$ (the standard Mises model). A general axially symmetric analysis has been presented by Hill (1976), for rigid/perfectly-plastic solids with the yield condition (6), over the entire range of $\lambda$.

Assuming that the plastic strain rates are normal to the yield surface and invoking the principle of plastic work equivalence we find that the flow rule associated with (6) is

$$\dot{\varepsilon}_r^P = \frac{\dot{\varepsilon}_P}{\sigma_e}\left[\frac{3}{4\lambda^2}(\sigma_r-\sigma_\theta) - \frac{1}{2}\left(\sigma_z - \frac{\sigma_r+\sigma_\theta}{2}\right)\right] \tag{7a}$$

$$\dot{\varepsilon}_\theta^P = \frac{\dot{\varepsilon}_P}{\sigma_e}\left[-\frac{3}{4\lambda^2}(\sigma_r-\sigma_\theta) - \frac{1}{2}\left(\sigma_z - \frac{\sigma_r+\sigma_\theta}{2}\right)\right] \tag{7b}$$

$$\dot{\varepsilon}_z^P = \frac{\dot{\varepsilon}_P}{\sigma_e}\left(\sigma_z - \frac{\sigma_r+\sigma_\theta}{2}\right) \tag{7c}$$

where $\varepsilon_P$ is the effective plastic logarithmic strain (a known function of the effective stress $\sigma_e$), and the superposed dot denotes differentiation with respect to a timelike parameter.

The plane strain pattern implies, by the elastic incompressibility ($\nu = \frac{1}{2}$) constraint and (7c),

$$\sigma_z = \tfrac{1}{2}(\sigma_r + \sigma_\theta) \tag{8}$$

so that definition (6) is reduced to

$$\sigma_e = \frac{\sqrt{3}}{2\lambda}(\sigma_\theta - \sigma_r) \tag{9}$$

where we have assumed that $\sigma_\theta > \sigma_r$ along the entire loading history. It is worth mentioning that the Tresca definition of the effective stress is obtained from (9) with $\lambda = \sqrt{3}/2$. More generally, it is observed that the effective stress (9)—implied by the assumptions of axisymmetry, incompressibility and plain strain—is just the maximum shear stress rescaled by the orthotropy parameter $\lambda$. Substituting (8)–(9) back in (7a–b) gives the plane strain constitutive relations

$$-\dot{\varepsilon}_r^P = \dot{\varepsilon}_\theta^P = \frac{\sqrt{3}}{2\lambda}\dot{\varepsilon}_P. \tag{10}$$

The elastic branch of the strain rates if given by the known Hookean relations; it follows that the total strain rates are given by

$$-\dot{\varepsilon}_r = \dot{\varepsilon}_\theta = \frac{\sqrt{3}}{2}\left(\lambda\dot{\Sigma} + \frac{\dot{\varepsilon}_P}{\lambda}\right) \quad \text{with } \Sigma = \frac{\sigma_e}{E} \tag{11}$$

or, after integrating from the initial stress free configuration,

$$-\varepsilon_r = \varepsilon_\theta = \frac{\sqrt{3}}{2}\left(\lambda\Sigma + \frac{\varepsilon_P}{\lambda}\right). \tag{12}$$

Turning to equilibrium requirements we have the single equation

$$\sigma_r' + \frac{1+u'}{r+u}(\sigma_r - \sigma_\theta) + \rho\omega^2(r+u)(1+u') = 0 \tag{13}$$

where $\rho$ is the material density. This can be rewritten, with the aid of (1)–(3) and (9), as

$$\mathrm{d}\sigma_r + \rho\omega^2 r\,\mathrm{d}r = \frac{2}{\sqrt{3}}\lambda\sigma_e\,\mathrm{e}^{-2\varepsilon_\theta}\frac{\mathrm{d}r}{r}. \tag{14}$$

A further substitution of (5) in (14) gives, with the use of (12),

$$\mathrm{d}\sigma_r + \tfrac{1}{2}\rho\omega^2\,\mathrm{d}(r^2) = -f(\Sigma)\,\mathrm{d}\sigma_e \tag{15}$$

where

$$f(\Sigma) = \frac{\Sigma\left(\lambda^2 + \dfrac{d\varepsilon_P}{d\Sigma}\right)}{\exp\left[\sqrt{3}\left(\lambda\Sigma + \dfrac{\varepsilon_P}{\lambda}\right)\right] - 1}. \tag{16}$$

Denoting by $(a, b)$ the undeformed inner and outer radii, respectively, we have the two boundary conditions

$$\sigma_r(r = a) = -p, \quad \sigma_r(r = b) = 0. \tag{17}$$

Integrating now eqn (15) and using the boundary data (17) we find that

$$\frac{p}{E} + \frac{\rho\omega^2}{2E}(b^2 - a^2) = \int_{\Sigma_b}^{\Sigma_a} f(\Sigma)\, d\Sigma \tag{18}$$

where $(\Sigma_a, \Sigma_b)$ are the boundary values of the nondimensionalized effective stress. A second equation follows from the exact integral of (5), namely,

$$\left(\frac{b}{a}\right)^2 = \frac{e^{\sqrt{3}\Delta_a} - 1}{e^{\sqrt{3}\Delta_b} - 1} \tag{19}$$

where $\Delta$ is the apparent total effective strain defined by

$$\Delta = \lambda\Sigma + \frac{\varepsilon_P}{\lambda} \tag{20}$$

and $(\Delta_a, \Delta_b)$ are the corresponding boundary values of $\Delta$.

An illuminating observation, suggested by a reviewer, is that the r.h.s. of (18) can be recast into the form

$$\int_{\Sigma_b}^{\Sigma_a} f(\Sigma)\, d\Sigma = \int_{\lambda\Sigma_b}^{\lambda\Sigma_a} \frac{(\lambda\Sigma)\dfrac{d\Delta}{d(\lambda\Sigma)}\, d(\lambda\Sigma)}{\exp(\sqrt{3}\Delta) - 1}.$$

This is identical with the version given by Durban (1979) for the pressurized Mises tube with the transformation $\Sigma \to \lambda\Sigma$ and $\varepsilon_p \to \varepsilon_p/\lambda$. With the same transformation eqn (18) agrees with the corresponding result by Lo and Abeyaratne (1981) for the rotating Mises tube. It can be concluded that if $\lambda$ remains constant along the loading path, orthotropy manifests itself only through the transformation of the uniaxial ($z$-direction) stress-strain curve to the in-plane shear stress-strain curve.

Equations (18)–(19) can be solved without difficulty, with any given data of $p$ and $\omega$, to determine the values of the effective stress at the inner and outer radii. With that solution in hand we get the radial stress profile, from (15),

$$\frac{\sigma_r}{E} = -\frac{p}{E} - \frac{\rho\omega^2}{2E}(r^2 - a^2) - \int_{\Sigma_a}^{\Sigma} f(\Sigma)\, d\Sigma \tag{21}$$

while the radial variation of the apparent effective strain is obtained from (5), (12) and (20) as

$$\left(\frac{r}{a}\right)^2 = \frac{e^{\sqrt{3}\Delta_a} - 1}{e^{\sqrt{3}\Delta} - 1}. \tag{22}$$

Combining that relation with definition (20), and recalling that $\varepsilon_P$ is a known function of $\Sigma$, we can easily determine the radial distribution of the effective stress. The circumferential stress component is then obtained from (9), and the radial displacement follows from (1) and (12).

Note that while no definite yield point has been introduced in the analysis, it is possible to use any piecewise description of the true stress–true strain relation through the appropriate form of (16).

The error introduced by the assumption of elastic incompressibility may be expected to remain small. This has been demonstrated in Durban (1988) where the pressurized tube is analysed for the compressible Mises solid with the finite strain deformation theory; the effect of retaining the actual Poisson ratio is virtually negligible over the practical range of radii ratios. Even for extremely thick walls there is an error of just a few percent, in the results for the bursting pressure, when elastic compressibility is neglected.

## THIN-WALL APPROXIMATIONS

The analysis presented so far covers a range of plastic-orthotropic solids that include the isotropic Tresca ($\lambda = \sqrt{3}/2$) and Mises ($\lambda = 1$) materials as particular cases. It would be instructive therefore, before proceeding with the general solution, to assess the effect of the orthotropy parameter $\lambda$ on the plastic strength of the tube. To this end we employ the usual thin-wall approximations along the lines presented in Durban (1979).

Denoting through-thickness averages by the subscript 0, we find from (18)–(19) the consistent first order expansions

$$\frac{p}{E} + \frac{\rho\omega^2}{2E}(b^2 - a^2) = f(\Sigma_0)(\Sigma_a - \Sigma_b) \tag{23}$$

$$\left(\frac{2}{\sqrt{3}}\right)\frac{b^2 - a^2}{b^2 + a^2} = \left(\frac{e^{\sqrt{3}\Delta_0}}{e^{\sqrt{3}\Delta_0} - 1}\right)\left(\frac{d\Delta}{d\Sigma}\right)_0(\Sigma_a - \Sigma_b). \tag{24}$$

These equations may be combined to give, with the aid of (16) and (20), the non-dimensionalized connection

$$P + \left(\frac{\beta^2 - 1}{2}\right)\Omega^2 = \frac{2}{\sqrt{3}}\left(\frac{\beta^2 - 1}{\beta^2 + 1}\right)\lambda\Sigma_0 e^{-\sqrt{3}\Delta_0} \tag{25}$$

where

$$P = \frac{p}{E} \quad \Omega^2 = \frac{\rho\omega^2 a^2}{E} \quad \beta = \frac{b}{a}. \tag{26}$$

Relation (25) provides the working value of the average effective stress $\Sigma_0$ for any permissible pair of loads $(P, \Omega)$. Of particular interest however is the failure criterion which is obtained from (25) when the r.h.s. reaches a maximum. Using definition (20) we find that this will happen when

$$\sqrt{3}\Sigma_0\left(\lambda^2+\left.\frac{d\varepsilon_P}{d\Sigma}\right|_0\right)=\lambda. \tag{27}$$

Neglecting the elastic strains and taking the pure power law characteristic $\varepsilon_P = K\Sigma^n$, where $(K, n)$ are material constants, we get from (27) the critical effective stress

$$\Sigma_0^{cr}=\left(\frac{\lambda}{\sqrt{3}nK}\right)^{1/n}. \tag{28}$$

The corresponding failure condition follows from (25) as

$$P+\left(\frac{\beta^2-1}{2}\right)\Omega^2=\frac{2}{\sqrt{3}}\left(\frac{\beta^2-1}{\beta^2+1}\right)(\sqrt{3}\,e)^{-1/n}\lambda^{(n+1)/n}\Sigma_u \tag{29}$$

where $\Sigma_u = (nK)^{-1/n}$ is the ultimate (necking) stress in uniaxial ($z$-direction) tension. It is clearly seen from (29) that increasing the orthotropy parameter $\lambda$ will cause an increase in the plastic failure strength of the tube. This is in agreement with the role of $\lambda$ in (20) since higher values of $\lambda$ reduce the relative contribution of the plastic branch. In the vicinity of the Mises model ($\lambda = 1$) we have with $\lambda = 1+\bar{\lambda}$, where $\bar{\lambda} \ll 1$, that

$$\lambda^{(n+1)/n}\approx 1+\left(1+\frac{1}{n}\right)\bar{\lambda} \tag{30}$$

indicating a relatively small coupling between the orthotropy shift $\bar{\lambda}$ and $n$, particularly for higher values of $n$.

When each loading component acts separately we recover from (29) the maximum (bursting) pressure

$$P_{\max}=\frac{2}{\sqrt{3}}\left(\frac{\beta^2-1}{\beta^2+1}\right)(\sqrt{3}\,e)^{-1/n}\lambda^{(n+1)/n}\Sigma_u \tag{31}$$

and the maximum angular speed

$$\Omega_{\max}^2=\frac{4}{\sqrt{3}}\left(\frac{1}{\beta^2+1}\right)(\sqrt{3}\,e)^{-1/n}\lambda^{(n+1)/n}\Sigma_u. \tag{32}$$

Note that for vanishingly thin tubes, with $\beta \to 1$, (32) approaches the finite limit

$$\Omega_L^2=\frac{2}{\sqrt{3}}(\sqrt{3}\,e)^{-1/n}\lambda^{(n+1)/n}\Sigma_u. \tag{33}$$

Each of the failure conditions (29) is described, for a given value of $\beta$, by a straight line in the $(P, \Omega^2)$ plane. The envelope formed by these (tangent) lines may be regarded as the performance curve of the tube since it sets a bound on all attainable values of the pair $(P, \Omega)$ at failure.

To obtain an explicit expression for the performance curve we equate to zero the partial derivative of (29) with respect to $\beta^2$, namely

$$\Omega^2=\frac{4}{(\beta^2+1)^2}\Omega_L^2. \tag{34}$$

Inserting (34) back in (29) gives

$$P = \left(\frac{\beta^2 - 1}{\beta^2 + 1}\right)^2 \Omega_L^2. \tag{35}$$

Relations (34)–(35) provide the parametric representation of the performance curve. Eliminating $\beta^2$ between (34) and (35) we get the simple explicit equation of the parabola

$$P = (\Omega_L - \Omega)^2 \tag{36}$$

with $\Omega \leqslant \Omega_L$.

Since $\Omega_L$ from (33) increases with $\lambda$ we may conclude that the extent of the performance domain bounded by (36) will also increase with $\lambda$. The validity of relation (36) is restricted to thin walled tubes and may be expected to be reliable in the range of $\beta < 2$.

Of course, a complete analysis of the instability condition will require a bifurcation study along the axisymmetric equilibrium path investigated here. Work of this kind for rotating disks has been presented by Storåkers (1977) and by Tvergaard (1978). The proper form of the instability condition under combined loading has been discussed in a recent paper by Hill (1988). While it is true that loss of stability may occur before or after maximum load is reached, the present finite strain analysis is of its own merit in exposing the nature of the primary equilibrium path.

## NUMERICAL EXAMPLES AND COMPARISON WITH EXPERIMENTS

Sample calculations of the failure lines, as determined by (18)–(19), were performed for aluminum 7075 T6 with the following specifications:

$$\varepsilon_P = K\Sigma^n; \quad E = 7.24 \cdot 10^{10} \frac{N_e}{m^2}, \quad K = 3.94 \cdot 10^{21}, \quad n = 10.9 \tag{37}$$

(Poisson's ratio of this material is $\nu = 0.32$ but in the present analysis, where elastic compressibility has been neglected, we take the value of $\nu = 0.5$).

The numerical procedure employed here is identical with the one described in Durban (1979); with a given value of $\beta = b/a$ it is an easy matter to find the maximum value of the integral on the r.h.s. of (18). That maximum, denoted by $P_{\max}$, is of course the bursting pressure $(p_{\max}/E)$ of the same tube in the absence of rotation. Thus, with the notation of (26) we get from (18) the failure lines of thick walled tubes as

$$P + \left(\frac{\beta^2 - 1}{2}\right)\Omega^2 = P_{\max}. \tag{38}$$

Some representative results for the performance envelopes, are shown in Fig. 1 for different values of the orthotropy parameter $\lambda$. Again, it is seen that the plastic strength of the tube increases with $\lambda$. It can be verified that the thin wall approximation (36), which for that particular material takes the form

$$P = (9.17 \cdot 10^{-2} \lambda^{0.546} - \Omega)^2 \tag{39}$$

remains in close agreement with the exact results for $\beta < 2$. Approximation (39) is valid for low values of $P$ and becomes increasingly conservative as $\Omega$ decreases.

We turn now to a comparison between our theoretical predictions and the experimental measurements given in Larsson *et al.* (1982) for the bursting pressure of aluminum and copper tubes. The uniaxial ($z$-direction) stress–strain characteristics for these metals are represented by

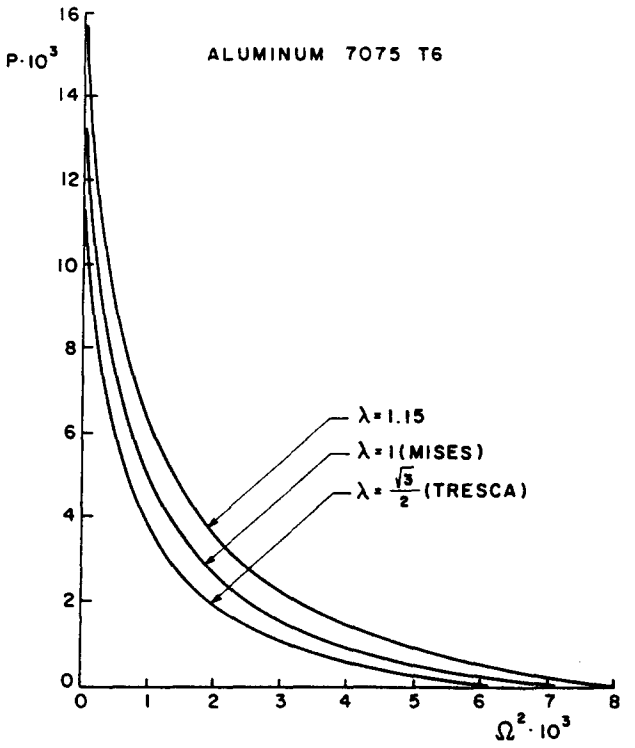


Fig. 1. Performance envelopes for aluminum 7075 T6.

$$\varepsilon = \Sigma \quad \text{for } \Sigma \leqslant \Sigma_Y \quad \text{with } \Sigma_Y = \frac{Y}{E}$$

$$\varepsilon = \Sigma + A_1(\Sigma - \Sigma_Y)^{n_1} + A_2(\Sigma - \Sigma_Y)^{n_2} \quad \text{for } \Sigma \geqslant \Sigma_Y \tag{40}$$

where $Y$ is the yield stress and $(A_1, A_2, n_1, n_2)$ are material constants. The specific values reported in Larsson *et al.* (1982) are

Aluminum:

$$\Sigma_Y = 0.952 \cdot 10^{-3} \quad E = 69.3 \cdot 10^3 \text{ MPa} \quad \nu = 0.3$$
$$A_1 = 104.9 \quad A_2 = 3.12 \cdot 10^{48} \quad n_1 = 1.18 \quad n_2 = 17.6 \tag{41}$$

Copper:

$$\Sigma_Y = 3.02 \cdot 10^{-4} \quad E = 116 \cdot 10^3 \text{ MPa} \quad \nu = 0.33$$
$$A_1 = 155.2 \quad A_2 = 1.203 \cdot 10^{11} \quad n_1 = 1.1 \quad n_2 = 4.58. \tag{42}$$

(Note however that the value of $\nu = 0.5$ has been used in the calculations.)

Figures 2 and 3 show the measured values of the bursting pressure $P_{max}$ for different radii ratios $\beta$. These experimental data are compared with theoretical results obtained from (18), with $\omega = 0$, and (19) for different values of the orthotropy parameter $\lambda$. Deviations of theoretical predictions based on the Mises model ($\lambda = 1$) from experimental data were attributed in Larsson *et al.* (1982) to material inhomogeneity and anisotropy induced by the tube forming process.

While little improvement on the Mises model ($\lambda = 1$) has been found for aluminum (Fig. 2), there is a very nice agreement for the copper tubes (Fig. 3) with $\lambda = 0.92$. It is interesting that the experimental results for copper are bounded (Fig. 3) between the Tresca ($\lambda = \sqrt{3}/2$) and Mises ($\lambda = 1$) models. For the aluminum (Fig. 2) the Tresca model still provides a lower bound on the bursting pressure, but deviations from the Mises model, or

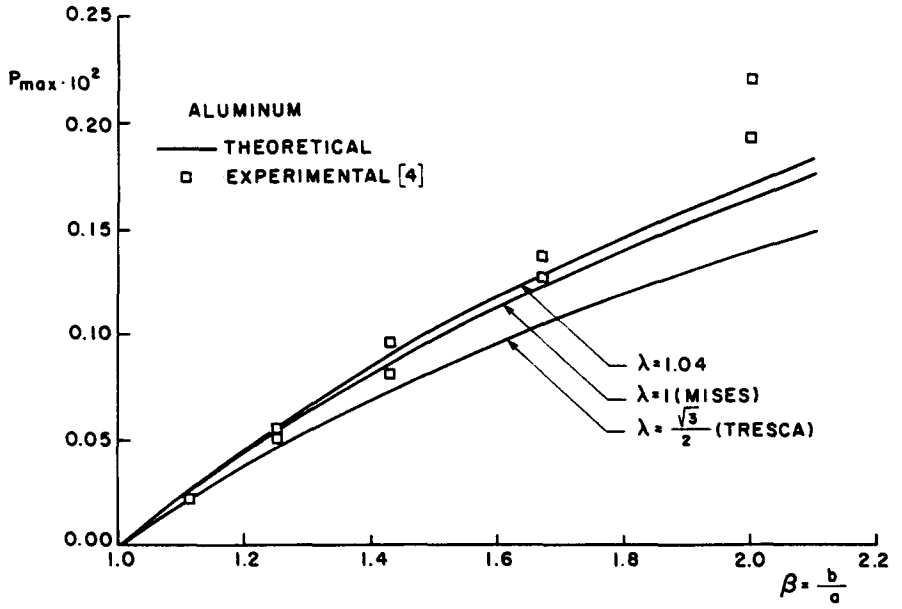


Fig. 2. The bursting pressure for aluminum tubes.

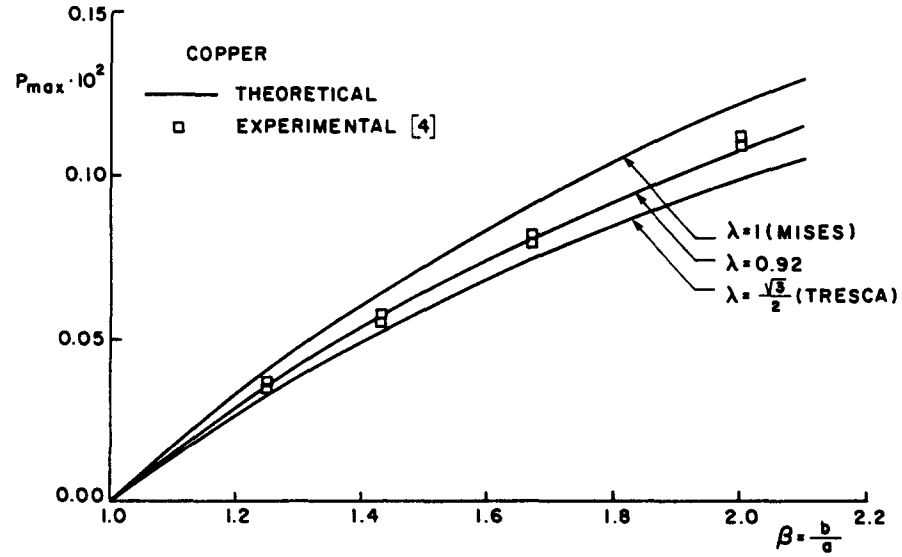


Fig. 3. The bursting pressure for copper tubes.

for that matter, the $\lambda = 1.04$ model, become appreciably large for thick tubes. It is worth mentioning in this context that the aluminum tubes used in the experiments by Larsson *et al.* (1982) were not annealed before testing. It is likely therefore that material inhomogeneity could have influenced the values of the bursting pressure shown in Fig. 2.

## FURTHER ANALYTICAL RESULTS

Despite the highly nonlinear nature of the governing system (18)–(19) it is still possible to extract some useful analytical results.

Consider first the elastic/perfectly-plastic solid at the onset of full plastification. The effective stress is then uniformly equal to $\Sigma_Y$ throughout the body, and the total effective plastic strain $\varepsilon_p$ vanishes at the outer radius. The integral on the r.h.s. of (18) is then transformed, with the aid of (16), to

$$\int_0^{\varepsilon_{Pa}} \frac{\Sigma_Y \, d\varepsilon_P}{\exp\left[\sqrt{3}\left(\lambda\Sigma_Y + \frac{\varepsilon_P}{\dot{\lambda}}\right)\right] - 1} \tag{43}$$

where $\varepsilon_{Pa}$ is the value of $\varepsilon_P$ at the inner wall. This integral admits a closed form expression and (18) becomes accordingly

$$P + \left(\frac{\beta^2 - 1}{2}\right)\Omega^2 = \frac{\lambda\Sigma_Y}{\sqrt{3}} \ln \frac{1 - e^{-\sqrt{3}\Delta_a}}{1 - e^{-\sqrt{3}\lambda\Sigma_Y}}. \tag{44}$$

Equation (19) here is reduced to

$$e^{\sqrt{3}\Delta_a} = 1 + \beta^2(e^{\sqrt{3}\lambda\Sigma_Y} - 1). \tag{45}$$

Combining (44) with (45) we obtain the failure line

$$P + \left(\frac{\beta^2 - 1}{2}\right)\Omega^2 = \frac{\lambda\Sigma_Y}{\sqrt{3}} \ln \frac{\beta^2 e^{\sqrt{3}\lambda\Sigma_Y}}{1 + \beta^2(e^{\sqrt{3}\lambda\Sigma_Y} - 1)} \tag{46}$$

which, for a given radii ratio, depends only on the single material parameter $\lambda\Sigma_Y$.

In the absence of internal pressure, for very thin tubes, with $\beta \to 1$, we obtain from (46) by a straightforward expansion the finite angular speed

$$\Omega_L^2 = \frac{2}{\sqrt{3}} \lambda\Sigma_Y e^{-\sqrt{3}\lambda\Sigma_Y} \tag{47}$$

which may be compared with (33).

To obtain the plastification envelope generated by the family of lines (46) we equate to zero the partial derivative of (46) with respect to $\beta^2$, resulting in

$$\Omega^2 = \frac{\frac{2}{\sqrt{3}}\lambda\Sigma_Y}{\beta^2[1 + \beta^2(e^{\sqrt{3}\lambda\Sigma_Y} - 1)]}. \tag{48}$$

Relations (48) and (46) provide the parameteric equations of the plastification envelope. The latter can be cast into the form

$$P + \left(\frac{\beta^2 - 1}{2}\right)\Omega^2 = \frac{\lambda\Sigma_Y}{\sqrt{3}} \ln\left[\beta^4\left(\frac{\Omega}{\Omega_L}\right)^2\right]. \tag{49}$$

It is possible to solve (48) for $\beta^2$ and insert the result in (49) to obtain an explicit equation for the complete plastification curve, viz.

$$\beta^2 = \frac{\sqrt{1+4e^{\sqrt{3}\lambda\Sigma_Y}(e^{\sqrt{3}\lambda\Sigma_Y}-1)\left(\frac{\Omega_L}{\Omega}\right)^2}-1}{2(e^{\sqrt{3}\lambda\Sigma_Y}-1)}. \tag{50}$$

Typical plastification envelopes, as evaluated from (49)–(50), are shown in Fig. 4 for different values of $\lambda\Sigma_Y$.

A more refined analysis—skipped here due to its algebraic complexity—shows that failure of the tube occurs before the onset of complete plastification. However, over the practical range of material properties and tube geometry there is virtually no difference in the corresponding values of the internal pressure. The distinction between the two pressure levels along the loading path becomes noticeable only for very thick tubes.

Our next example is that of an elastic/linear-hardening material within the framework of small strain plasticity. The uniaxial stress strain curve is given by

$$\varepsilon = \Sigma \quad \text{for } \Sigma \leqslant \Sigma_Y$$

$$\varepsilon = \Sigma_Y + \frac{1}{\eta_t}(\Sigma - \Sigma_Y) \quad \text{for } \Sigma \geqslant \Sigma_Y \tag{51}$$

where $\eta_t = E_t/E$ and $E_t$ stands for the constant tangent modulus. The total plastic strain in the post-yield range follows as:

$$\varepsilon_P = \varepsilon - \Sigma = \left(\frac{1-\eta_t}{\eta_t}\right)(\Sigma - \Sigma_Y) \quad \text{for } \Sigma \geqslant \Sigma_Y. \tag{52}$$

For small strains it is permissible to use the approximation

$$e^{\sqrt{3}\Delta} \approx 1 + \sqrt{3}\Delta. \tag{53}$$

Thus, at the onset of complete plastification in the tube we can write the integral on the r.h.s. of (18) in the form

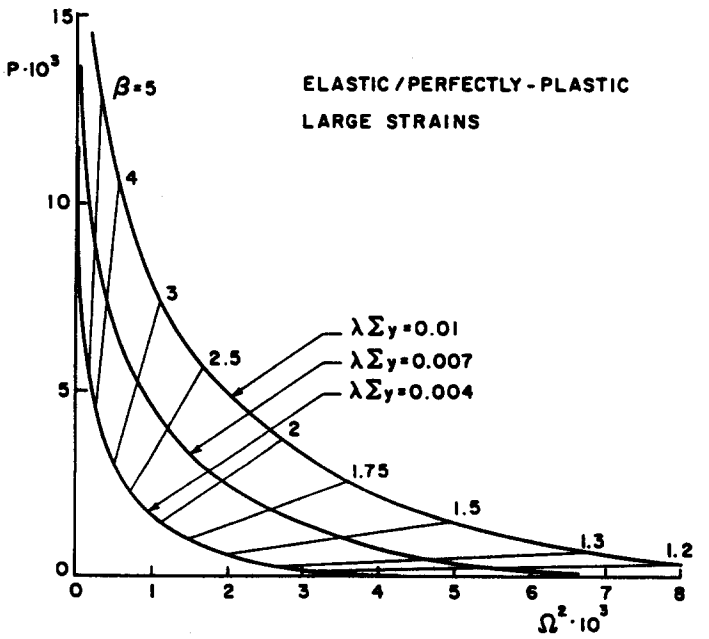


Fig. 4. Complete plastification envelopes for elastic/perfectly-plastic materials.

$$\frac{1}{\sqrt{3}}(1+\Lambda)\int_{\Sigma_Y}^{\Sigma_a}\frac{\Sigma\,d\Sigma}{(1+\Lambda)\Sigma-\Sigma_Y}=\frac{1}{\sqrt{3}(1+\Lambda)}\left[(1+\Lambda)(\Sigma_a-\Sigma_Y)+\Sigma_Y\ln\frac{(1+\Lambda)\Sigma_a-\Sigma_Y}{\Lambda\Sigma_Y}\right] \tag{54}$$

where

$$\Lambda=\frac{\lambda^2\eta_t}{1-\eta_t}. \tag{55}$$

Similarly, eqn (19) is reduced to

$$\beta^2=\frac{(1+\Lambda)\Sigma_a-\Sigma_Y}{\Lambda\Sigma_Y}. \tag{56}$$

It follows that the full plastification lines are given by

$$P+\left(\frac{\beta^2-1}{2}\right)\Omega^2=\frac{\Omega_L^2}{2(1+\Lambda)}[\Lambda(\beta^2-1)+\ln\beta^2] \tag{57}$$

where

$$\Omega_L^2=\frac{2}{\sqrt{3}}\lambda\Sigma_Y \tag{58}$$

is the limiting angular speed for a rotating, thin-walled, tube with no internal pressure. This definition coincides of course with the small strain version of (47).

The complete plastification envelope is obtained, by the usual technique, from the parameteric relations

$$\Omega^2=\frac{\Omega_L^2}{1+\Lambda}(\Lambda+\beta^{-2}) \tag{59}$$

$$P=\frac{\Omega_L^2}{2(1+\Lambda)}(\ln\beta^2-1+\beta^{-2}). \tag{60}$$

That analysis is restricted to small strains—implying an increasing error as the tube becomes thicker. The plastification envelopes, illustrated in Fig. 5, are nevertheless illuminating in

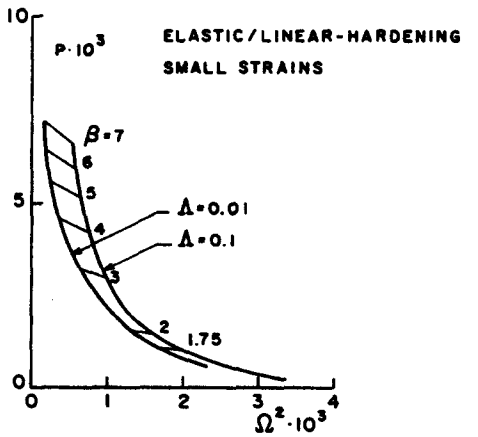


Fig. 5. Complete plastification envelopes for elastic/linear-hardening materials. Small strain solution.

reflecting the coupling—through parameter $\Lambda$—between plastic orthotropy and strain hardening.

## REFERENCES

Durban, D. (1979). Large strain solution for pressurized elasto/plastic tubes. *J. Appl. Mech.* **46,** 228–230.

Durban, D. (1988). Finite straining of pressurized compressible elasto-plastic tubes. *Int. J. Engng. Sci.* **26,** 939–950.

Hill, R. (1976). Plastic analysis of pressurized cylinders under axial load. *Int. J. Mech. Sci.* **18,** 145–148.

Hill, R. (1988). Path sensitivity of material response at intrinsic eigenstates in classical plasticity. *Math. Proc. Camb. Phil. Soc.* **103,** 371–381.

Larsson, M., Needleman, A., Tvergaard, V. and Storåkers, B. (1982). Instability and failure of internally pressurized ductile metal cylinders. *J. Mech. Phys. Solids* **30,** 121–154.

Lo, K. K. and Abeyaratne, A. (1981). Finite elastic-plastic deformation of a rotating hollow cylinder. *J. Appl. Mech.* **48,** 666–668.

Storåkers, B. (1977). On uniqueness and stability under configuration-dependent loading of solids with or without a natural time. *J. Mech. Phys. Solids* **25,** 269–287.

Tvergaard, V. (1978). On the burst strength and necking behaviour of rotating disks. *Int. J. Mech. Sci.* **20,** 109–120.